IET Renewable Power Generation

Research Article

IET Journals
The Institution of Engineering and Technology

Analysis and experimental validation of partial shading mitigation in photovoltaic system using integrated dc–dc converter with maximum power point tracker

ISSN 1752-1416
Received on 11th February 2019
Revised 15th May 2019
Accepted on 21st June 2019
E-First on 24th July 2019
doi: 10.1049/iet-rpg.2019.0188
www.ietdl.org

Mohd Zulkifli Ramli[1], *Zainal Salam*[2] ✉

[1]*Faculty of Electrical Engineering, Universiti Teknikal Malaysia Melaka, 76100 Durian Tunggal, Melaka, Malaysia*
[2]*School of Electrical Engineering, Faculty of Engineering, Universiti Teknologi Malaysia, 81310 Johor Bahru, Malaysia*
✉ *E-mail: zainals@utm.my*

Abstract: An integrated dc–dc converter with maximum power point tracker (IDCCM) is an electronic device that can be utilised to increase the output power of a photovoltaic generation system. Despite its potential benefits, there is an absence of a comprehensive analytical work to characterise the IDCCM performance under different partial shading conditions. Thus, this work proposes an analytical method to evaluate the system with IDCCM for different shading pattern/intensity, irradiance, and temperature. To validate the analysis, the SPV 1020 boost-type IDCCM devices are incorporated into a 2 kWp experimental test-rig. The performance of the IDCCM is benchmarked against the conventional system that utilises bypass diodes (alone). The results indicate that the IDCCM improves the performance of the central inverter as it ensures the latter consistently tracks the global peak. Also, it was found that that the performance of the IDCCM depends on the shading intensity: at low intensity, the IDCCM is able to extract energy from the shaded modules; however, it is ineffective at high shading intensity. Furthermore, when the shading is absent, the energy gained by the IDCCM is offset by the continuous power losses due to its internal operations.

1 Introduction

Despite the many advantages of the photovoltaic (PV) power generation, there are several issues of concern to system installers – one of them is the energy loss due to partial shading. This phenomenon occurs when certain parts of the array are shaded, while others are uniformly irradiated. Partial shading has to be strictly differentiated from low irradiance level. For the latter, the entire modules in the array experience low, but uniform irradiance. On the other hand, for the partial shading case, only certain modules are shaded; this results in low irradiance occurrence for certain spots while the remaining of the array retains higher irradiance. The main sources of partial shading are nearby structures, such as chimneys, poles, overhead power cables, transmission lines, and trees. The passing cloud, fallen leaves, and animal remains on the module surface are also possible causes of this condition. Sundareswaran *et al*. [1] estimated that 9% shading of the array surface can result in system-wide generation loss of over 50%. Since partial shading leads to possible module hot spot, bypass diodes are connected across to prevent damage.

Most of the installed PV systems are based on string/central inverters. In this configuration, a number of modules are connected in series and the combined dc output feeds the inverter. As a result, if one of the modules in the string is shaded, the performance of the system will be drastically affected. Moreover, to optimise the performance of the system, the modules must be identical and mounted at the same tilt angle. Despite these inherent disadvantages, the string inverter configuration is very popular because it offers the most attractive dollar per watt solution. Moreover, the inverter is normally housed in a safe place, i.e. protected from the harsh environment. In terms of electrical wiring, the system is relatively easy to install. The string arrangement also provides flexibility in terms of PV operating voltage [2–4].

During the normal condition, i.e. under the uniform irradiance, the P–V characteristic curve has a unique peak, known as the maximum power point (MPP). Thus, the conventional MPP tracker (MPPT) such as perturbed and observed (P&O), hill-climbing or incremental conductance can locate the MPP easily. However, when the module is partially shaded, its associated bypass diode turns on. This diode short-circuits the module and forces its voltage to be practically zero. As a consequence, its characteristics are transformed from a single to a multiple-peak curve [5–7]. Since the conventional MPPT is basically based on peak identification, the algorithm cannot discriminate between the global and local peaks. In most cases, it is trapped at the latter – resulting in power loss [8–10]. Several researchers have improved the conventional MPPT by incorporating additional intelligence to ensure consistent and accurate tracking of the global peak (GP) [7, 11]. Moreover, soft computing techniques such as particle swarm optimisation [12], artificial neural network [13], fuzzy logic [14], differential evolution [15], and cuckoo search [16] have been utilised to locate the GP using their multi-modal search capabilities.

Notwithstanding the above-mentioned efforts, it must be acknowledged that even if the MPPT successfully tracks the GP, the shaded module remains unusable in practice because its voltage is brought down to zero (as a result of the bypass diode action). However, there are certain portions of the module where the shading does not take place. Theoretically, these portions are still capable of generating the output power. One approach to extract this 'latent' energy is to use a small dc–ac converter, known as the micro-inverter. The device is connected underneath the module and its output is directly connected to the ac grid. Each micro-inverter has its own MPPT that independently tracks the MPP of its corresponding module. Owing to this one-to-one connectivity, whatever power available from the shaded module can be readily exported to the grid. Since the micro-inverter is a departure from the string configuration, the shaded module will not affect the non-shaded ones. Thus, it can suitably be used for systems with partial shading. Normally, the micro-inverter is rated at approximately the same power as the module itself.

Another method to harvest the power of the shaded module is to utilise a dedicated dc–dc converter – known as the integrated dc–dc converter with MPPT (IDCCM). In certain literature, this device is also referred to as the dc power optimiser. Similar to the micro-inverter, the IDCCM has its own MPPT controller; thus, the power from each module (including the shaded one) can be independently tracked. The main difference between the two is that, instead of

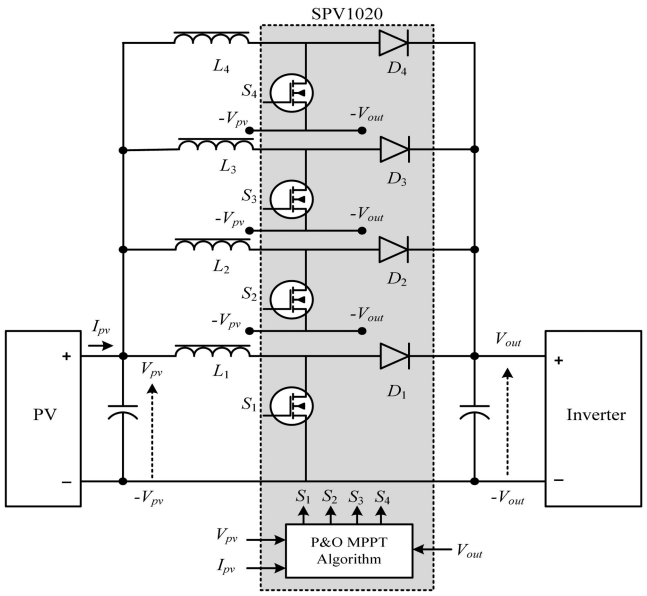

Fig. 1 *Architecture of the SPV 1020 IDCCM. The components in the shaded area are internal to the device*

directly connecting the IDCCM to the grid, several of these devices are connected in series – forming a string that is connected to an inverter [17–20]. Thus, the IDCCM improves the performance of the system by ensuring that the string current is not influenced by the shaded modules. Furthermore, since the power from the module is individually maximised by its MPPT, the output power extracted from the string is maximised too.

In comparison with a micro-inverter, the system with IDCCM exhibits several merits. As reported in [21], the overall system cost (which includes a central inverter) is 20–50% lower than the micro-inverter. Furthermore, since the system is based on the string inverter, the cost/watt of the system decreases as the installation size increases. In terms of the parts count, the IDCCM is about one-third less than a typical micro-inverter [21]. Fewer components suggest a lower failure rate and extended product life time. Besides that, the micro-inverter has other problems too. Since most micro-inverters are primarily based on a two-stage conversion, they require large electrolytic capacitors for dc link stabilisation. Unfortunately, the lifetime of an electrolytic capacitor greatly reduced when exposed to high temperatures. As a result, the reliability of the micro-inverter is reduced, as argued by Hasan *et al*. [22]. On the other hand, most IDCCM designs require low-value capacitors. Thus, the ceramic capacitors can be used instead, which is much more adaptable to high temperature. As far as the physical wiring is concerned, the system with IDCCM uses the standard PV cable. On the contrary, the micro-inverter requires an expensive trunk cable and dedicated ac load centre prior to the ac disconnect. Moreover, as the output of the IDCCM is dc, it can be also used for non-grid application such as the standalone PV system that utilises batteries.

Despite its increasing popularity, scientific publications related to IDCCM are very limited. The ones available are mainly focused on laboratory verification of the device characteristics [23–25]. To date, there is an absence of a comprehensive analytical work to characterise the IDCCM performance under different shading conditions. Such analysis is particularly useful during the design stage, as it improves the understanding of the system behaviour prior to installation. Acknowledging this literature gap, this work proposes an analytical method to predict and characterise the performance of the PV system with IDCCM. The analysis is based on the two-diode PV simulation model [26], which is developed using Matlab/Simulink tools. The validity of the analysis is verified by comparing the energy-time profile from a field (experimental) system to the analytical *P–V* curves. To benchmark the performance of the IDCCM, it is to evaluate against the system bypass diode (only).

The paper is organised in seven sections. The next section introduces the architecture of the SPV 1020 device (which is the IDCCM used in this work) and its interconnections with the modules and the central inverter. Next, the development of the simulation model of the PV system using the two-diode model is described. This is necessary because the analysis with IDCCM under partial shading is very complex; hence the need for simulation. In Section 4, the characteristic (behaviour) of the system under the uniform and partial shading is investigated. Three cases, namely the heavy-, medium- and low-shading conditions are considered. Section 5 describes the field set-up of the 2 kWp PV system. Then, the field measurements of the selected shading patterns are presented in Section 6. In Section 7, these results are corroborated with the analysis and simulation. The issue of the central inverter being trapped at the local peak is also highlighted here. In addition, several more scenarios with different shading patterns are presented. Finally, the paper is summarized based on the important findings obtained from the analysis, simulation, and field experiments.

2 Dc–dc converter with MPPT (IDCCM)

The IDCCM is an alternative solution for the partial shading problem using the hardware approach. In a typical installation, a number of IDCCM devices are connected in series and the combined dc output voltage feeds the central inverter (or to the battery, for the stand-alone system). This is in contrast to the micro-inverter, in which its ac output is directly connected to the grid. There are several dc–dc converter topologies that are used as the backbone for IDCCM; the most common ones are the boost, buck, and buck–boost. In terms of currently available products, there are two categories of IDCCM devices sold in the market. First is the partial IDCCM, where a set of basic dc–dc converter and MPPT controller is embedded inside the chip, while a number of less critical components are connected (by the user) outside the device. Examples of such devices are the SPV 1020 from the ST Microelectronics [23], SM 72441 from Texas Instrument [27] and the LT 8490 from Linear Technology [28]. This type of IDCCM is more flexible and as long as the output power rating is adhered to, the user can tailor the device performance to suit his needs. Second is the IDCCM sold as a complete functional chip. For this type, the entire device is integrated into a single chip, without the need for external components. Several manufactures are actively producing this product for various voltage and power ranges; two of the more prominent ones are the Alencon [29] and SolarEdge [30]. These chips are shipped as a complete package and no alteration can be done to tailor the device characteristics.

For the purpose of this work, the SPV 1020 IDCCM is utilised. It is a partial device and its basic circuit is shown in Fig. 1. The device is rated at 40 V, 300 W. Structurally, the SPV 1020 is based on a monolithic, four-phase, interleaved dc–dc boost converter. To achieve the interleave function, inductors (L_1–L_4), switches (S_1–S_4) and diodes (D_1–D_4) are duplicated thrice to form four parallel branches. The switches and diodes are integrated inside the device, while inductors and capacitors are added externally.

3 Simulation of the PV system

The proposed analytical work (for the PV system with IDCCM) is based on the two-diode equivalent circuit model [26]. The circuit is shown in Fig. 2. This is a well-known model that takes advantage of the accuracy and speed of simulation. The model contains the irradiation (G) and temperature (T) light-dependent PV current (I_{PV}) and the saturation current of the diodes (I_{o1} and I_{o2}). The output current is

$$I = I_{pv} - I_{o1}\left(exp\left(\frac{V+IR_s}{a_1V_{T1}}\right)-1\right) - I_{o1}\left(exp\left(\frac{V+IR_s}{a_2V_{T2}}\right)-1\right) - \left(\frac{V+IR_s}{R_p}\right) \quad (1)$$

where V_{T1} and V_{T2} are the thermal voltages of respective diodes, while a_1 and a_2 represent their ideality constants. The R_s and R_p are series and parallel resistances of the model, respectively. The relationship of I_{PV} with G and T can be written as

$$I_{PV} = (I_{PV\_STC} + K_I \Delta T)\frac{G}{G_{STC}} \tag{2}$$

In (2), I_{PV_STC} (in A) is the light generated current at the standard test condition (STC) ($G = 1000$ W/m^2, $T = 25$°C, pressure = 1.5 ATM), $\Delta T = T - T_{STC}$ (in K), G (in W/m^2) is the surface irradiance and G_{STC} is the irradiance at STC. The constant K_I is the short circuit current coefficient. As suggested in [26], a_1 is set to unity and a_2>1.2, while I_{o1} and I_{o2} are made equal. Thus

$$I_{o1} = I_{o2} = I_o = \frac{(I_{sc\_STC} + K_I \Delta T)}{\exp[(V_{oc,STC} + K_V \Delta T)/\{(a_1 + a_2)/p\}V_T] - 1} \tag{3}$$

4 Analysis using the two-diode model

4.1 Characteristics under uniform irradiance

From the PV model equations, the output current of the cell when connected to the IDCCM can be written as

$$I = \begin{cases} \text{Eq. (1)}, & 0 \le V_{IDCCM} \le V_{mp,} \\ \dfrac{P_{mp}}{V_{IDCCM}}, & V_{mp} \le V_{IDCCM} \le V_{lim.} \end{cases} \tag{4}$$

where V_{IDCCM} is the output voltage of the individual IDCCM device. Furthermore, V_{lim} is defined as the maximum IDCCM output voltage, while P_{mp} and V_{mp} are the power and voltage at the MPP of the array. To illustrate the IDCCM characteristics under uniform irradiance, a string that comprises eight Solar World SW 250 ploy-crystalline modules (PV1–PV8) is simulated. The specifications for the SW 250 at STC are given in Table 1. The interconnection of these eight modules (with SPV 1020) to the central inverter is shown in Fig. 3. For the partial shading test, two modules, namely PV7 and PV8 are deliberately shaded. They are compared to the normal system with bypass diodes. For convenience, the latter is abbreviated as BPD (system with bypass diode).

The red and blue traces in Fig. 4*a* are the *I–V* curves of the system with IDCCM and BPD, respectively. As is expected, the system with BPD exhibits the normal *I–V* shape, with the MPP voltage denoted by $V_{mp.}$ For the IDCCM, its *I–V* curve follows the same loci as the former, but only until V_{mp}. Beyond this point, it operates under the constant power mode – which is a typical characteristic for a dc–dc converter. Furthermore, the current falls abruptly to zero at V_{lim} due to the limitation of the SPV 1020 output power. The value of V_{lim} (296 V) is obtained by multiplying the maximum output voltage of the module (37 V) with the number of devices in the string (eight). Theoretically, if the output power capability of the IDCCM is >300 W, V_{lim} can be the extended beyond 296 V, as suggested by the dotted trace in Fig. 4*b*.

4.2 Characteristics under partial shading

The generalised *I–V* characteristic of the IDCCM under partial shading condition is shown in Fig. 4 [31]. Its output is given as

$$V_{IDCCM} = kV_{PV} \text{ where } 1 \le k \le k_{max} \tag{5}$$

In (5), k is the boost step-up ratio and V_{PV} is the output voltage of the module. The total output voltage generated by N number of IDCCM in series can be calculated using

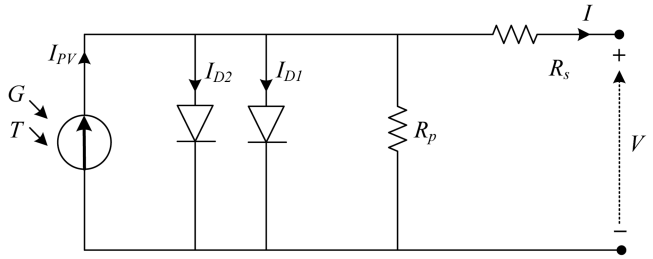

Fig. 2 *PV cell two-diode model [27]*

Table 1 Solar world SW250 specifications at STC

Parameter	Value
maximum power, P_{max}	250 W
open circuit voltage, V_{oc}	37.8 V
MPP voltage, V_{mpp}	31.1 V
short circuit current, I_{sc}	8.28 A
MPP current, I_{mpp}	8.05 A

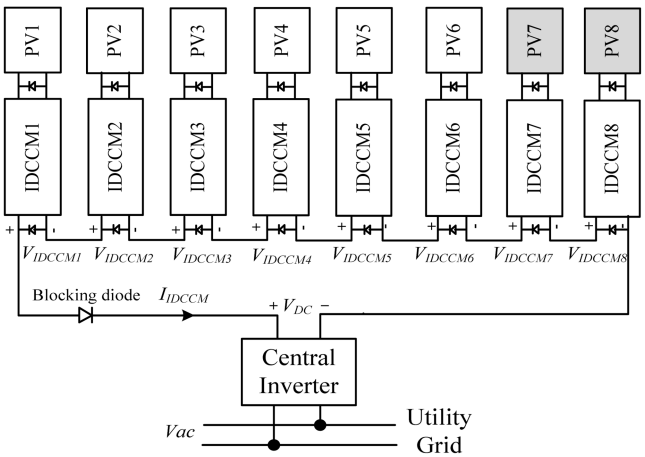

Fig. 3 *Interconnection of the IDCCM to the grid*

$$V_{DC} = kV_{mp}\left(1 + \sum_{i=1}^{N-1} \alpha_i\right), \tag{6}$$

where α_i is defined as the ratio of I_{PV} to the current at MPP for each module, i.e.

$$\alpha_i = k_i \frac{I_{PV}}{I_{mp}} \tag{7}$$

There are two flat regions in Fig. 5, i.e. Region(1) and Region(2) represent constant power. One important characteristic of IDCCM is that, once it operates at a particular peak, it locks itself in that position until a new peak is found [31]. In the case of two regions curve shown in Fig. 4, the higher Region(2) is bounded by V_{DCmax} and $V_{DCmin.}$ The values of V_{DCmax} and V_{DCmin} can be determined by

$$V_{DCmax} = k_{max} \times V_{mp}\left(1 + \sum_{i=1}^{N-1} \alpha_i\right) \tag{8}$$

and

$$V_{DCmin} = \frac{k_{min}}{\alpha_{low}} \times V_{mp}\left(1 + \sum_{i=1}^{N-1} \alpha_i\right) \tag{9}$$

where α_{low} is the lowest value of α among the modules. Thus, to extract the maximum power from a string of IDCCM, the input

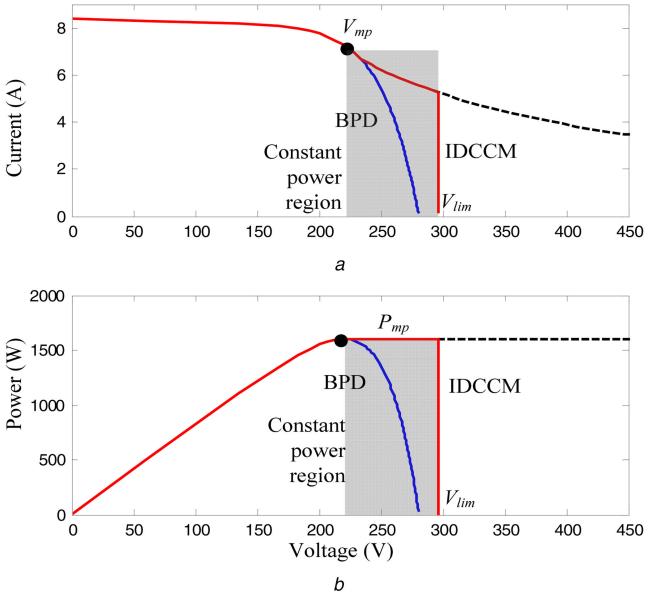

Fig. 4 *The characteristics of the photovoltaic systems*
(a) *I–V* characteristics of the system with BPD (blue) and IDCCM (red) under uniform irradiance, ***(b)*** *P–V* characteristics

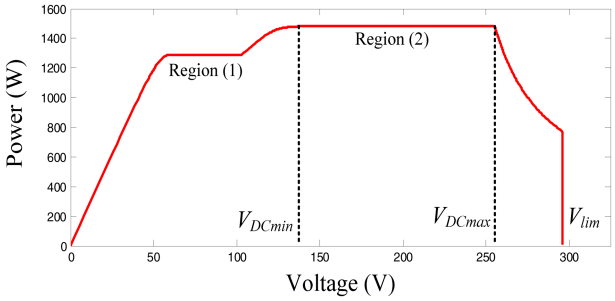

Fig. 5 *Generalised I–V curve under partial shading*

voltage window of the inverter (V_{DC}) is expected to operate between V_{DCmax} and V_{DCmin}.

The procedure to construct the *I–V* and *P–V* curves for the system with IDCCM is illustrated by the flow chart in Fig. 6. For convenience, the PV system with eight modules shown in Fig. 3 is used. Using $I_{IDCCM} = 0$ as the initial value, the output voltage of each IDCCM (V_{IDCCM1} to V_{IDCCM8}) is iteratively calculated using (1). The series output voltage (i.e. connected to the inverter, V_{DC}), is the sum of V_{IDCCM1} to V_{IDCCM8}. The computed values V_{DC} and I_{IDCCM} are plotted as a point on the *I–V* curve. In the next iteration, the value of I_{IDCCM} is incremented by 0.1 A. From here, a new value of V_{DC} is calculated and plotted. The process is repeated until I_{IDCCM} reaches its maximum value (I_{scNS}). The complete *I–V* curve is shown in Fig. 7*a*. The *P–V* curve is generated by multiplying I_{IDCCM} *and* V_{DC}, as shown in Fig. 7*b*.

Depending upon the intensity of the shading, the behaviour of the system with IDCCM can be categorised into three cases, as described below.

4.2.1 Case A: heavy (60%) partial shading: For this case, the shaded modules are operated with 60% shading. Note that 60% shading implies that only 40% of the irradiance is allowed to fall on the module. To illustrate its effect, simulation is carried out by shading two modules, i.e. PV7 and PV8, as shown in Fig. 3. The non-shaded modules are operated at $G = 1000$ W/m^2, while the shaded ones are at $G = 600$ W/m^2. To be more realistic, the module temperature (T) is set to 55°C.

Fig. 8*a* shows the *I–V* curve of the first six (non-shaded) modules, i.e. PV1–PV6. Two traces, i.e. system with IDCCM (red) and BPD (blue) are shown in the same graph. As can be seen, the characteristic curves for both are similar to the ones shown in

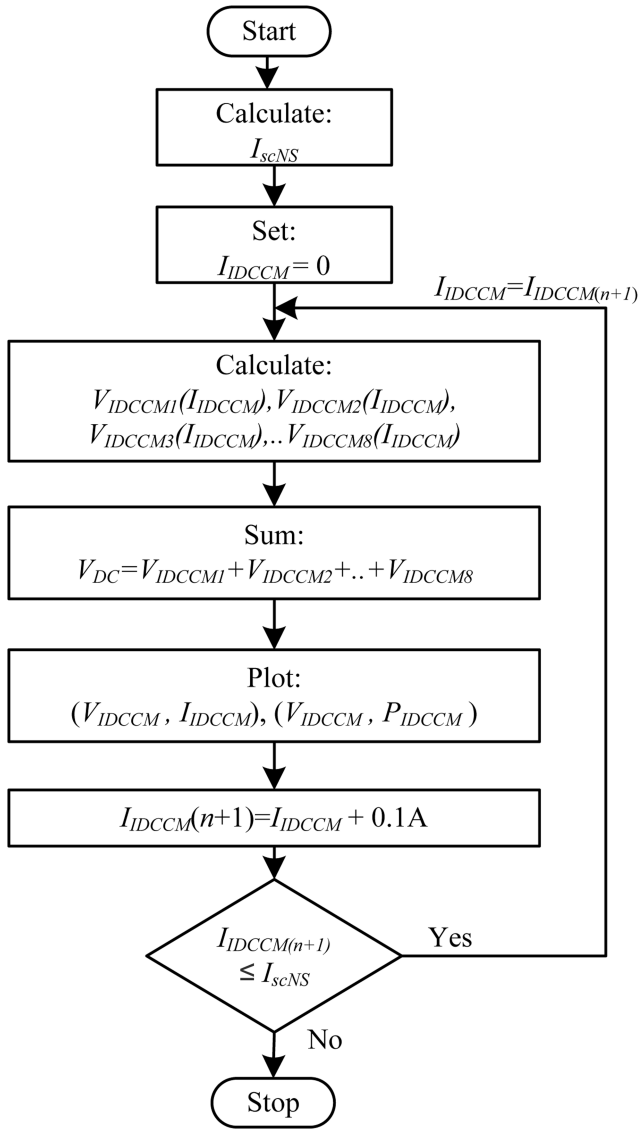

Fig. 6 *Flow chart to construct the I–V and P–V curves for the system with IDCCM*

Fig. 4. The MPP values (V_{mpNS}, I_{mpNS}) are 164 V and 8.3 A, respectively. The short circuit current for the non-shaded modules (I_{scNS}) is calculated to be 9.5 A. Note that this value is higher than the I_{sc} given in the datasheet (i.e. 8.28 A at STC), due to the higher module temperature (55°C). As shown earlier, prior to the MPP, the *I–V* curve of the IDCCM follows the BPD curve. Then, it enters the constant power region. At V_{limNS} (222 V) the current drops abruptly from 6.1 to 0 A. Fig. 8*b* shows the *I–V* curves for the two heavily shaded modules, i.e. PV7 and PV8. Using similar notation, the short circuit current of the shaded modules (I_{scS}) is 3.84 A, while the MPP (V_{mpS}, I_{mpS}) is at 48.9 V and 3.2 A. The value of V_{limS} is 74 V. At this point, I_{limS} drops from 2.1 A to 0.

When the eight modules are connected (as in Fig. 3), the voltage summation results in the waveform as shown in Fig. 8*c*. The *I–V* curve of the system with BPD exhibits the well-known staircase current waveform. Its MPP voltage and current (V_{mp}, I_{mp}) remain at the region 164–220 V and 8.3 A, respectively. On the other hand, the IDCCM does not appear to extract the power from the shaded modules. The reason for this unexpected behaviour can be explained as follows. From the current waveform in Fig. 8*c*, it can be observed that up until MPP, the output power is generated by the non-shaded modules only, i.e. the shaded modules are not contributing to the output power. This is due to $I_{scS} < I_{limNS}$. The difference in the current value forces the bypass diodes across the IDCCM7 and IDCCM8 to be turned on, clamping their output voltages to zero. The corresponding *P–V* curves are shown in

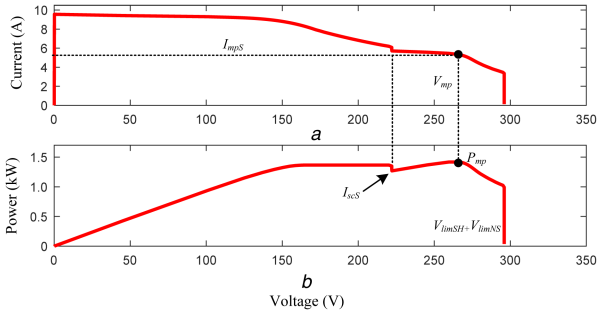

Fig. 7 *Characteristics of the PV system with IDCCM*
(a) *I–V* curve, ***(b)*** *P–V* curve

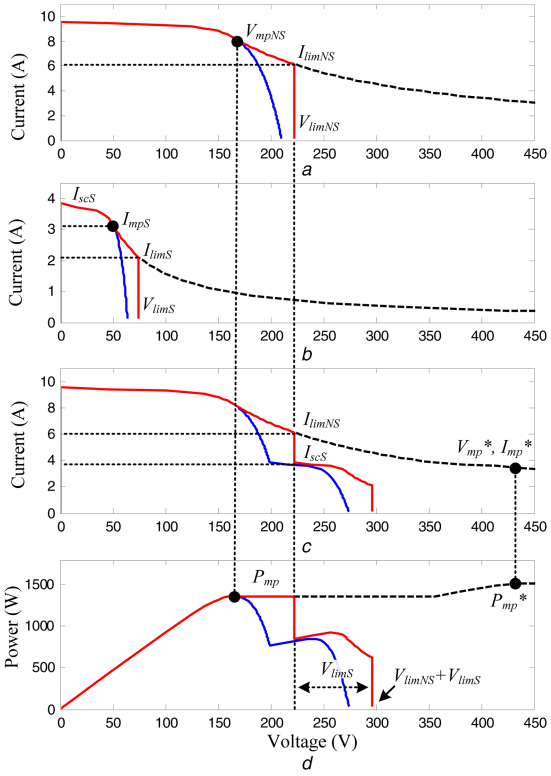

Fig. 8 *Simulated I–V and P–V curves for case A (heavy shading). Red trace: IDCCM; blue: BPD*
(a) *I–V* curve of six unshaded modules in series, ***(b)*** *I–V* curves of two shaded modules, ***(c)*** *I–V* curve after voltage summation, ***(d)*** Corresponding *P–V* curve

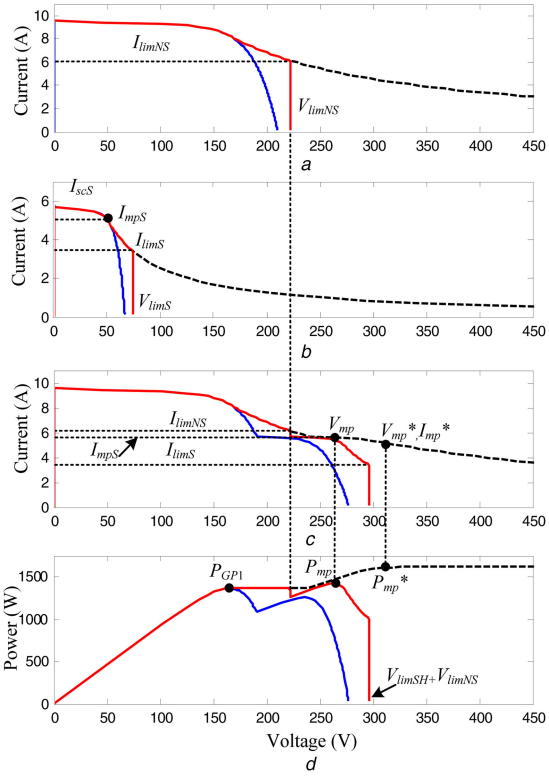

Fig. 9 *Simulated I–V and P–V curves for case B (medium shading). Red trace: IDCCM, Blue: BPD*
(a) *I–V* curve of six unshaded modules in series, ***(b)*** *I–V* curves of two shaded modules, ***(c)*** *I–V* curve after voltage summation, ***(d)*** Corresponding *P–V* curve

Fig. 8*d*. As envisaged, the P_{mp} that can be achieved by the IDCCM is the same as the BPD. This analysis suggests that for heavy shading condition, the IDCCM does not offer any advantage over the system with bypass diode.

4.2.2 Case B: medium (40%) partial shading: For this case, the shading intensity of PV7 and PV8 is reduced to 40%. This implies that 60% of the irradiance is allowed to hit the module surface. Fig. 9*a* shows the *I–V* curve of both systems for the first six modules, i.e. PV1–PV6. Since no change is made, the characteristic is similar to *case A*. Fig. 9*b* depicts the *I–V* curve that corresponds to the two shaded modules. Using the same notation, V_{limS} is 74 V, while I_{scS} and I_{limS} are 5.7 and 3.4 A, respectively. Once the eight modules are connected in series, the resulting *I–V* and *P–V* curves are shown in Figs. 9*c* and *d*, respectively. As can be seen, the system with IDCCM exhibits a higher GP (P_{mp}), compared to the BPD (P_{GP1}). Furthermore, it can be observed that up until V_{limNS}, the power is contributed by the non-shaded modules only – similar to case A. In this region, PV7 and PV8 output power are zero due to $I_{scS} < I_{limNS}$. However, after V_{limNS}, the bypass diode is no longer activated because the current is less than I_{scS}. Consequently, the tracking algorithm of the IDCCM identifies the peak at P_{mp}. Furthermore, it can be observed that the abrupt drop in the IDCCM current occurs at $V_{limS} + V_{limNS}$. Beyond this point, the current is zero due to the limitation in the IDCCM output voltage. Nevertheless, if the IDCCM with a higher output power is used, the actual GP should be located along the dotted line, i.e. at P_{mp}*.

4.2.3 Case C: light (20%) partial shading: In this case, 80% of the irradiance is allowed to hit the module surface. Fig. 10*a* shows the *I–V* curves of the first six non-shaded modules. Expectedly, they are similar to the previous cases. Additionally, the *I–V* curve for the two shaded modules (PV7 and PV8) is shown in Fig. 10*b*. Note that V_{limS} is maintained at 74 V. However, due to the light shading, I_{scS} and I_{limS} increase to 6.9 and 4.20 A, respectively. The resultant *I–V* curve for the combination of the eight modules is shown in Fig. 10*c*. Interestingly, the system with IDCCM exhibits similar *I–V* characteristics to the system with BPD, i.e. staircase-like current. This can be attributed to the fact that in the case of light shading, I_{scS} is always larger than I_{limNS}. As a result, none of the shaded modules operates under short circuit condition. Unlike cases A and B, the IDCCM is now able to extract all the available power from these two modules. This is proven in Fig. 10*d*,

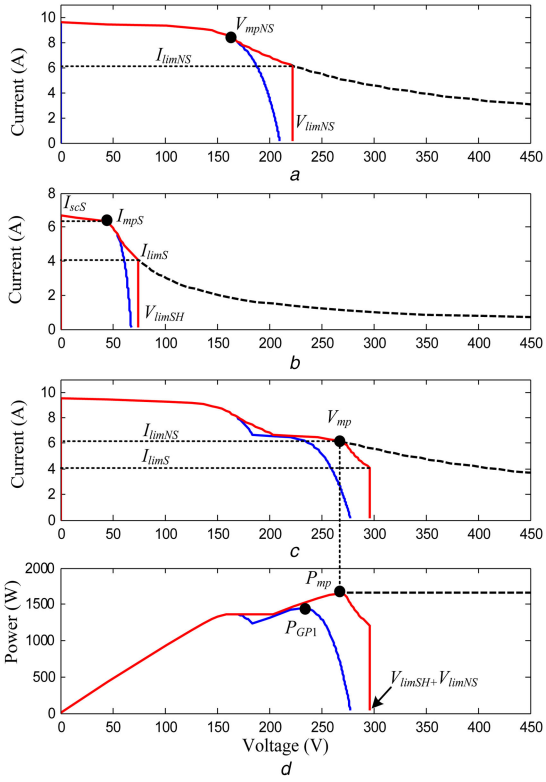

Fig. 10 *Simulated I–V and P–V curves for case C (light shading). Red trace: IDCCM; blue: BPD*

(a) *I–V* curve of six unshaded modules in series, ***(b)*** *I–V* curves of two shaded modules, ***(c)*** *I–V* curve after voltage summation, ***(d)*** Corresponding *P–V* curve

whereby the highest power harvested by the system with IDCCM is P_{mp}. Note that, any further increase in voltage will not affect the location of P_{mp}.

5 Experimental validation

5.1 Field system set-up

The experimental verification is based on the actual field data obtained from a 2 kWp PV system. The photograph of the set-up and a single unit of the IDCCM board are shown in Fig. 11. Similar to simulation, the array comprises two strings; each with eight SW 250 modules, specified earlier in Table 1. Furthermore, to maximise the energy yield, both the IDCCM and BPD systems are mounted on a two-axis tracker, which rotates from east to west. The Solar World 2000HF grid-connected central inverter is used to convert the PV power to ac. The inverter is rated at 2.5 kW, while its MPP window ranges from 175 to 480 V. In the default condition, the modules are in full exposure to the sun, i.e. all modules in the string are not shaded.

To emulate the partial shading phenomena, the targeted modules are manually covered by acrylic films with various shading levels. The variation in the shading is achieved by super-imposing the acrylic film with a semi-transparent paper. The intensity of shading is measured by the percentage of reduction in the short circuit current (I_{SC}) at a particular temperature. A higher percentage means that the shading is more intense, which implies that the shaded module receives less light penetration. For consistency, three intensity levels are used, namely 20% for light (L), 40% for medium (M) and 60% for heavy (H) shading. The data is captured using a data logger at five-second intervals. The voltage, current and power measurements are measured using the highly accurate PM6000 power analyser from Voltech Instruments. The irradiance is measured using the secondary standard pyranometer model CMP11 from Campbel Scientific. The temperature is measured by using the PT 100 thermocouple.

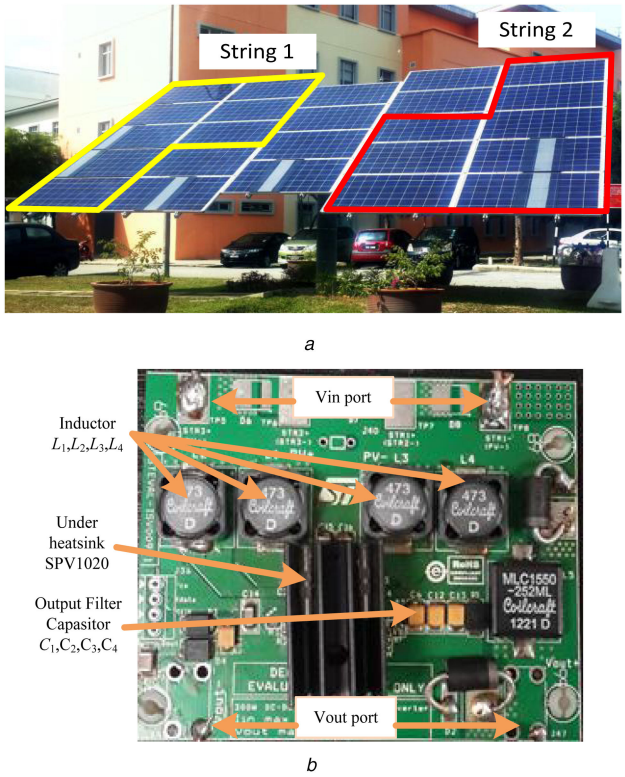

Fig. 11 *The experimental set-up photographs*

(a) Experimental set-up. String 1: the system with IDCCM, String 2: the system with BPD, ***(b)*** Photograph of the standard single unit IDCCM board

5.2 Imposed shading pattern

Table 2 shows the shading pattern imposed on the eight modules (PV1–PV8) over a 10-h daytime duration (from 8.00 am to 7.00 pm). The shading pattern and intensity levels are chosen to be generic, i.e. it could be the combination of multiple large objects such as buildings, poles, and trees. The data is logged starting at hour 8:00. Initially, none of the modules is shaded. Starting from hour 11:30, the shadows are introduced by placing the acrylic sheets as described in the previous section. At hour 17:00, all acrylic sheets are removed.

6 Results

For convenience, the profiles (i.e. snapshots of the waveforms for a specific period) of the PV output power (P), irradiance (G) and temperature (T) are divided by several time slots – based on the change in the shading condition imposed by Table 2. These measured quantities are compared to the *P–V* curve obtained from the analytical work in Section 3.

6.1 Hours 08:00–11:30

This is the condition prior to any shading. From the P profiles shown in Fig. 12, it can be observed that the power obtained from the system with BPD is slightly higher than the IDCCM. This is expected because the internal circuitry of the latter continuously draws a small amount of power to maintain its operation. On the contrary, for the system with BPD, the diodes are not activated under uniform irradiance condition; hence it does not experience such losses.

6.2 Hours 11:30–13:00

When the medium level shading is introduced to PV3 and PV4 at hour 11:30, almost immediately the power levels for both systems drop. However, the system with IDCCM is able to retain higher power because its individual MPPT controller ensures that whatever available energy from the shaded module is extracted. To determine the energy gain by the IDCCM, one particular operating

Table 2 Shading pattern for the eight modules

Panel no.	Time (24 h)																			
	9		10		11		12		13		14		15		16		17		18	
PV1	—	—	—	—	—	—	—	—	—	—	—	—	—	—	—	—	—	—	—	—
PV2	—	—	—	—	—	—	—	—	—	—	—	—	—	—	—	—	—	—	—	—
PV3	—	—	—	—	—	M	M	M	M	H	H	H	H	H	H	H	—	—	—	—
PV4	—	—	—	—	—	M	M	M	M	M	M	M	M	L	L	L	—	—	—	—
PV5	—	—	—	—	—	—	—	—	—	M	M	M	M	—	—	—	—	—	—	—
PV6	—	—	—	—	—	—	—	—	—	—	—	—	—	—	—	—	—	—	—	—
PV7	—	—	—	—	—	—	—	—	—	—	—	—	—	—	—	—	—	—	—	—
PV8	—	—	—	—	—	—	—	—	—	—	—	—	—	—	—	—	—	—	—	—

M is medium, H is heavy, L is low shading.

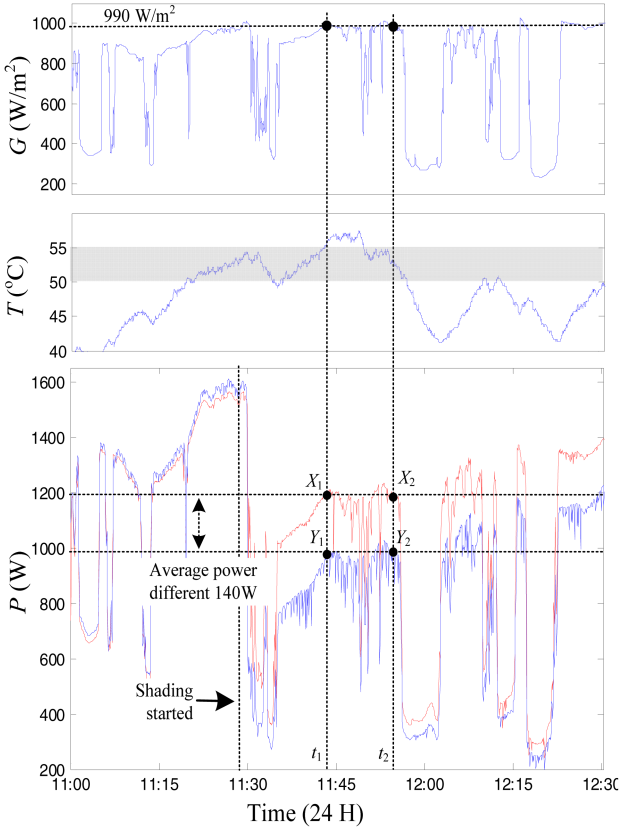

Fig. 12 *Profiles of G, T, and P for 11:00 to 12:30. Shading is introduced at hour 11:30. Blue trace: system with BPD; red trace: with IDCCM*

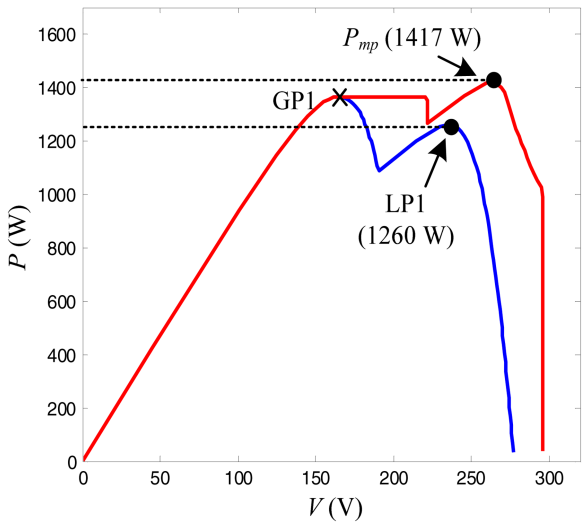

Fig. 13 *P–V curves for hours 11:30 to 13:30 for G = 990 W/m² and T = 52.5°C. Blue trace: the system with BPD; red trace: system with IDCCM*

irradiance ($G = 990$ W/m^2) is arbitrarily selected. It can be seen, for that particular G, several values of T are possible. Thus, a temperature range, i.e. 50° C < T < 55° C is allowed. This is shown in Fig. 12 by the shaded band on the T profile. Within this band, eight different time instants that intersect $G = 990$ W/m^2 are marked. The corresponding P of the system with IDCCM and BPD for the eight selected points are X_1, X_2,..., X_8 and Y_1, Y_2,…,Y_8, respectively. To avoid the cluttering of the graph, only two instants, i.e. t_1 and t_2 are marked in Fig. 12. These two points correspond to X_1 and X_2 (as well as Y_1 and Y_2) in the P profile. By taking the average of the eight data points, the calculated power difference between the system with IDCCM and BPD is 140 W.

The analytical P–V curve is used to validate the measured data. To maintain consistency, the same G (990 W/m^2) values are used. The T is selected to be the average, i.e. 52.5°C. The plotted P–V curves for the system with IDCCM and BPD are shown in Fig. 13. As can be seen, the difference power between the two is 164 W. Thus, the validity of the measured data is acceptable – considering the fact that the practical system exhibits a certain amount of losses attributed to the inverter efficiency, cable ohmic losses, dust and module mismatch [32, 33]. Furthermore, it is interesting to note that for the IDCCM, the shape of the I–V curve resembles case B. This result is consistent with the medium shading pattern imposed on PV3 and PV4 for this duration.

6.3 Hours 13:30–15:30

At hour 13:30, the shading intensity level for PV3 is increased from M to H, while PV4 remains at M. Furthermore, another module, i.e. PV5 is shaded at M. The snapshots of the G, T and P profiles for hours 13:15 to 13:45 are shown in Fig. 10. Again, the G is chosen as 990 W/m^2 and the temperature range is 50–55°C. The P–V curves are constructed for the same value of G and T = 52.5°C. These curves are shown in Figs. 14 and 15, The measured power difference between the system with IDCCM and BPD increases to 311 W. This is in agreement with the theoretical P–V curve, i.e. 355 W. Furthermore, by observing the I–V curve, it can be identified that the system with IDCCM operates in case B.

6.4 Hours 15:30–17:00

At hour 15:30, the shading intensity for PV4 is reduced from M to L. In addition, the shading for PV5 is totally removed. From the profile shown in Fig. 16, the average difference in power is 487 W. The measurement is made at $G = 600$ W/m^2 and 45 < T < 50°C. The temperature is set to a slightly lower range due to the lesser heating effect of the late afternoon sun. The analytical P–V curves for G = 600 W/m^2 and T = 45.5°C are shown in Fig. 17. The measured power is consistent with simulated results, i.e. 520 W. The IDCCM is operating in case C.

7 Discussions

7.1 Central inverter trapped at a local peak

Despite the good agreement between the field and analytical data, a huge jump in the measured power gain is observed at hour 13:30.

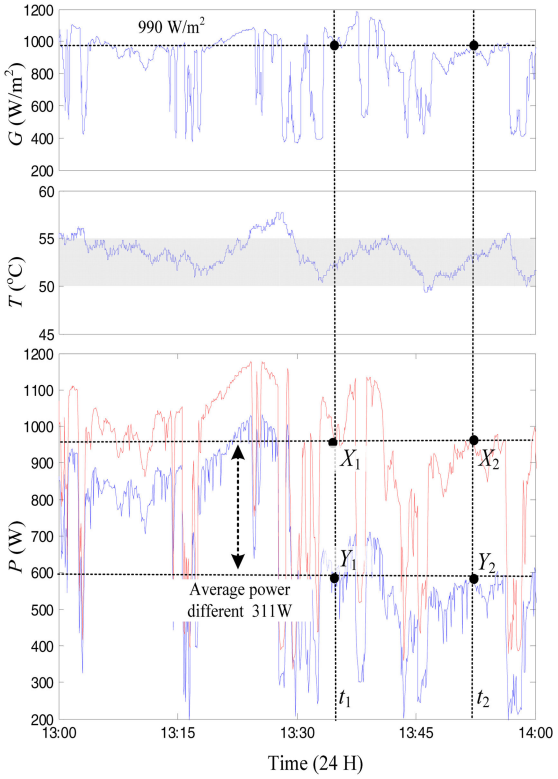

Fig. 14 *Profiles of G, T, and P for hours 13:00 to 13:50. Change of shading is introduced at hour 11:30. Blue trace: system with BPD; red trace: system with IDCCM*

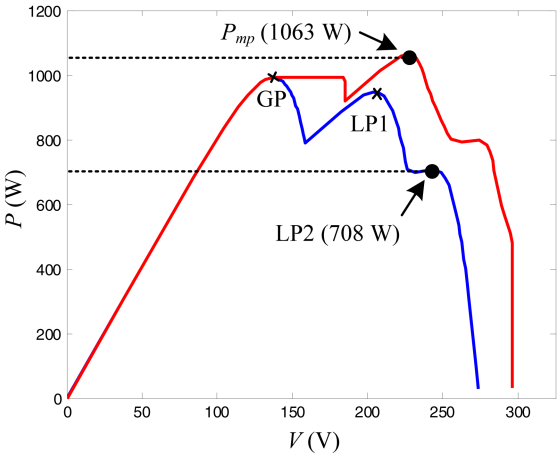

Fig. 15 *P–V curve between hours 13:30 to 15:30. Shaded modules: PV3 = H, PV5 = M, PV6 = M. Red trace: system with BPD; blue trace with IDCCM*

The (average) power increases rapidly from 140 to 311 W. Although a higher difference is expected, the large gain (171 W) cannot be justified by the inclusion of two additional shaded modules. Similarly, a large jump (487 W) is observed between at hour 15:30. These irregularities need clarification.

Further investigation reveals that the power difference between the system with IDCCM and BPD is not solely due to the ability of the former to extract more energy from the shaded module. It appears that in the BPD mode, the central inverter is forced to operate at the lowest local peak. This hypothesis is verified by measuring the operating voltage of the inverter from hours 13:00 to 14:00. As shown in Fig. 18, this voltage ranges from 235 to 245 V. If the *P–V* curve in Fig. 15 is referred, this voltage is in the vicinity of the lowest local peak, i.e. LP2 (242 V). Since the voltage for the GP is 125 V, it can be suggested that the central inverter indeed tracks LP2, instead of the GP. This is because, if the correct GP is tracked, the power difference should be only 88 W (1063–975 W). The same can be said for the power jump at hour 15:30. As can be

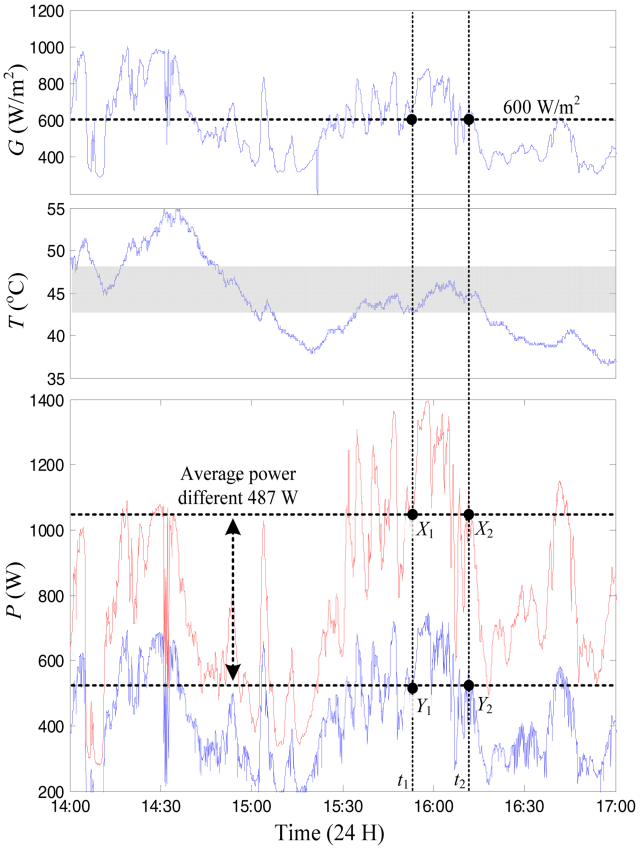

Fig. 16 *Instantaneous power between hours 14:00 and 17:00. Shading is changed at hour 15:30. Blue trace: system with BPD, red trace: with IDCCM*

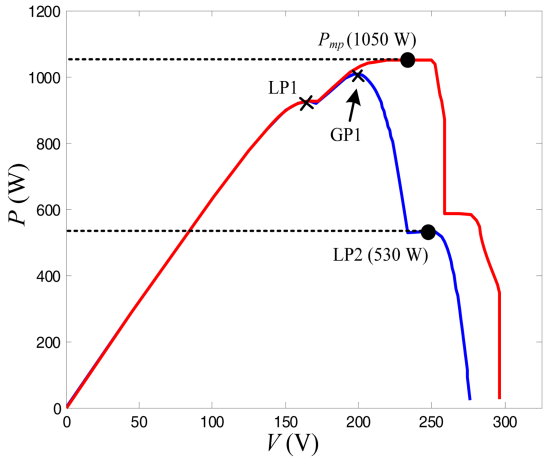

Fig. 17 *P–V curve between hours 15:30 and 17:00. Shaded modules PV3 = H, PV4 = L. Red trace: system with BPD; blue trace: with IDCCM*

seen from Fig. 17, the inverter is trapped at a local peak (LP2). On the other hand, the system with IDCCM always tracks the GP correctly.

7.2 Cumulative energy gain

The cumulative energy yield for the 10 h duration is plotted in Fig. 19. Prior to the initiation of the partial shading, the energy accumulated from the system with BPD is ~3.3% higher than the IDCCM. This is due to the internal power losses that are incurred by the latter under the uniform irradiance condition. However, when the shading is introduced (at hour 11:30), the energy gap is gradually reduced; by the end of the 10 h, the energy yield is 3.9 and 5.4 kWh for the BPD and IDCCM, respectively – an increase of 38%.

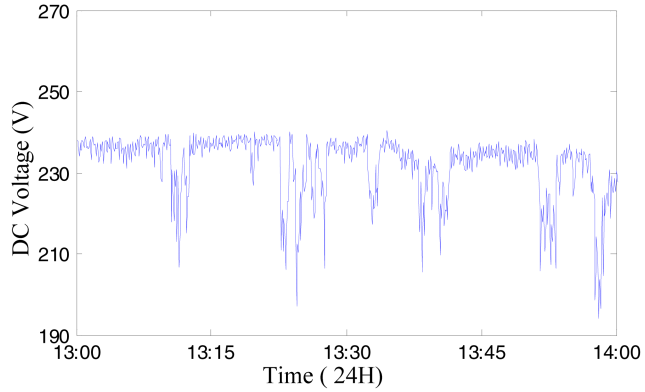

Fig. 18 *Input dc voltage profile of the system with BPD to show that the central inverter operates at the local peak, LP2*

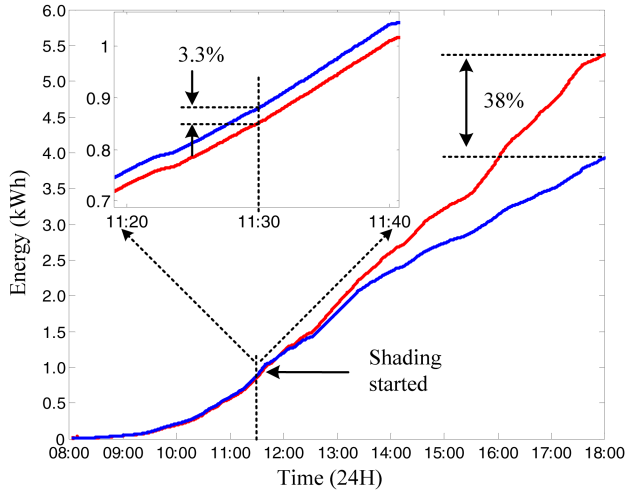

Fig. 19 *Field result for total energy yield. Blue trace: system with BPD, red trace: system the IDCCM*

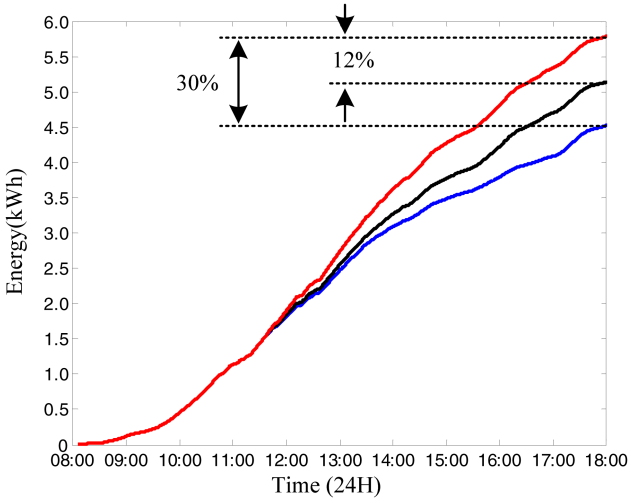

Fig. 20 *Simulation of total energy yield. Red trace: IDCCM; black trace: BPD with inverter tracking GP; blue trace: BPD with inverter tracking local peak*

However, as pointed out in Section 6.1, the significant portion of the energy difference can be attributed to the inability of the central inverter to track GP in the BPD mode. It is interesting to examine what would happen if the inverter is allowed to track the GP, instead of the local peak. The finding will reflect the system performance if a better inverter (i.e. able to track the GP) is installed. For this purpose, an analysis is carried out for the system with the BPD under the following conditions: (i) when the inverter tracks the GP and (ii) when it tracks the (lowest) local peak. For comparison, the system with IDCCM is also simulated. To maintain consistency, the same shading pattern, i.e. as in Table 2 is imposed.

Fig. 20 shows the simulated energy yield for the 10-h duration. The output power computation is based on their corresponding P–V curves, i.e. Figs. 13, 15 and 17. As is expected, the system with the IDCCM generated the highest output. For the system with BPD, when the central inverter is trapped at the local peak, the output power is ∼30% lower than the IDCCM. This is in agreement with the field results shown in Fig. 19. However, if the central inverter is allowed to continuously track the GP, the yield is increased. As can be observed, the energy yield is 12% lower than the case with the IDCCM. Thus, it can be confirmed that a significant drop in the energy is indeed due to the tracking deficiency of the central inverter. Nevertheless, the gain of energy by installing IDCCM is still considerable.

7.3 Other shading patterns

Since the cumulative energy yield depends on the shading pattern and intensity, as well as the irradiance and temperature profiles, it is expected that the performance of the IDCCM varies for different shading conditions. In addition, the peak tracking capability of the central inverter also plays an important role because under certain partial shading condition, the inverter may not be able to track the GP correctly. Although it is difficult to quantify the results in a general way (due to the unlimited permutations of shading patterns), it is possible to make certain conclusions by observing the trend of energy yield. This is an acceptable approach because the main objective is to evaluate the relative performance of the system with IDCCM and BPD, not the absolute results. Table 3 depict the various shading conditions imposed on the system over a 10-h period. For the first three cases, the array is subjected to single intensity: (a) heavy (H), (b) medium (M) and (c) low (L). The purpose is to validate the analysis of the system with IDCCM for case A (H), case B (M), and case C (L). The remaining two cases are mixed patterns (of different intensities), chosen arbitrarily.

Table 3 Other shading patterns imposed on the modules

Panel no.	Hour of the day-time (24 h)									
	9	10	11	12	13	14	15	16	17	18
(a) pattern no. 1										
PV1	—	—	—	—	—	—	—	—	—	—
PV2	—	—	—	H	H	H	H	H	—	—
PV3	—	—	—	H	H	H	H	H	—	—
PV4	—	—	—	—	—	—	—	—	—	—
PV5	—	—	—	—	—	—	—	—	—	—
PV6	—	—	—	—	—	—	—	—	—	—
PV7	—	—	—	—	—	—	—	—	—	—
PV8	—	—	—	—	—	—	—	—	—	—
(b) pattern no. 2										
—	—	—	—	—	—	—	—	—	—	—
PV1	—	—	—	—	—	—	—	—	—	—
PV2	—	—	—	M	M	M	M	M	—	—
PV3	—	—	—	M	M	M	M	M	—	—
PV4	—	—	—	—	—	—	—	—	—	—
PV5	—	—	—	—	—	—	—	—	—	—
PV6	—	—	—	—	—	—	—	—	—	—
PV7	—	—	—	—	—	—	—	—	—	—
PV8	—	—	—	—	—	—	—	—	—	—
(c) pattern no. 3										
—	—	—	—	—	—	—	—	—	—	—
PV1	—	—	—	—	—	—	—	—	—	—
PV2	—	—	—	L	L	L	L	L	—	—
PV3	—	—	—	L	L	L	L	L	—	—
PV4	—	—	—	—	—	—	—	—	—	—
PV5	—	—	—	—	—	—	—	—	—	—
PV6	—	—	—	—	—	—	—	—	—	—
PV7	—	—	—	—	—	—	—	—	—	—
PV8	—	—	—	—	—	—	—	—	—	—
(d) pattern no. 4										
PV1	—	L	M	M	M	L	—	—	—	—
PV2	—	—	L	M	M	—	—	—	—	—
PV3	—	—	L	L	L	—	—	—	—	M
PV4	—	—	—	—	—	—	—	—	M	M
PV5	—	—	—	—	—	—	M	M	M	M
PV6	—	—	—	—	—	—	—	—	—	—
PV7	—	—	—	—	—	—	—	—	—	—
PV8	—	—	—	—	—	—	—	—	—	—
(e) pattern no. 5										
PV1	—	—	—	L	L	M	M	M	—	—
PV2	—	—	—	M	H	H	H	L	—	—
PV3	—	—	—	L	M	M	H	—	—	—
PV4	—	—	—	—	L	L	M	—	—	—
PV5	—	—	—	—	—	—	—	—	—	—
PV6	—	—	—	—	—	—	—	—	—	—
PV7	—	—	—	—	—	—	—	—	—	—
PV8	—	—	—	—	—	—	—	—	—	—

M is medium, H is heavy, L is low shading.

For pattern no. 1, there is almost no energy gain, as shown in simulation results in Table 4. The GP IDCCM and BPD are at the same power level. This is consistent with the analysis for heavy shading, as explained in Section 4.2.1. However, the field data (also shown in the same table) indicate that the power yield IDCCM is slightly lower than BPD. This is due to the fact that the former experiences internal power loss during its operation, as noted earlier. For pattern no. 2, the simulated energy gain by IDCCM is 2.12%, while for pattern no. 3, it is 5.47%. These findings are consistent with the analysis that states that the IDCCM is more effective during the low-shading condition. This simulation result is supported by the respective field data, shown in Table 4 (2.01, 4.55%, respectively). For pattern no. 4, the heavy shading is not present; therefore for every hour, IDCCM extracts more power from the shaded modules. Additionally, since more modules are being shaded, the simulated energy gain by the IDCCM increases to 6.10%. For pattern no. 5, the energy is lower (5.54%) due to heavy shading imposed on PV2 and PV3.

In general, the IDCCM extracts energy during light and medium shading. For heavy shading, however, its advantage diminishes; in fact, the yield is lower than BPD due to the internal losses. The results also confirm that the analysis presented in this study is valid and thus can be used to predict the performance of the PV system connected to IDCCM.

Table 4 Results of the partial shading test for patterns shown in Table 3. (Field: field data; Sim: simulation)

Pattern no.	Yield using BPD (kWh)		Yield using IDCCM (kWh)		Gain in Energy (%)	
	Field	Sim.	Field	Sim.	Field	Sim.
1	8342	8668	8421	8668	−0.91	0.00
2	8669	9001	8843	8810	2.01	2.12
3	9693	9860	10,135	10,400	4.55	5.47
4	8475	8501	8971	9020	5.85	6.10
5	7918	8120	8328	8570	5.17	5.54

8 Conclusions

This work provides a thorough analysis of the PV system fitted with the IDCCM during the partial shading. The field results from 2 kWp PV systems indicate that the IDCCM improves energy yield when the PV system is subjected to certain shading patterns over several hours of operation. These results are well predicted by the analysis. However, the superiority of the IIDCCM cannot be generalised due to two important observations. First, in the absence of partial shading, the IDCCM always draw current from the module to sustain its operation – resulting in continuous internal power losses and hence reduced efficiency. This factor is not considered in the analysis. Second, as confirmed by the experiments, in a certain situation, the large power difference between IDCCM and BPD is partly due to the inability of the central inverter to track the GP correctly. Probably, the installed inverter utilises normal P&O or hill climbing MPPT algorithm, which lacks the ability to track the GP under partial shading. If these two factors are discarded, it can be concluded that overall, the proposed analytical method provides a good estimation of the system performance with IDCCM.

9 Acknowledgments

This work is funded by the Ministry of Higher Education, Malaysia under the Malaysia Rising Star Award grant. It is managed by Universiti Teknologi Malaysia (UTM) under Vot. No. R.J130000.7823.4F919. It is also partially funded by Prototype Short Term Research Grant, Universiti Teknikal Malaysia Melaka (UTEM) under project no: PJP/2013/FKE/PROTOTAIP/S01282.

10 References

[1] Sundareswaran, K., Vignesh Kumar, V., Palani, S.: 'Application of a combined particle swarm optimization and perturb and observe method for MPPT in PV systems under partial shading conditions', *Renew. Energy*, 2015, **75**, pp. 308–317

[2] Duo, L., Zhe, Z., Biwen, X., *et al.*: 'A method of power decoupling for long life micro-inverter'. IECON 2011 – 37th Annual Conf. on IEEE Industrial Electronics Society, Melbourne, Australia, 2011, pp. 802–807

[3] Ramli, M., Salam, Z.: 'A simple energy recovery scheme for to harvest the energy from shaded photovoltaic modules during partial shading', *IEEE Trans. Power Electron.*, 2014, **29**, pp. 6458–6471

[4] Balog, R.S., Yingying, K., Uhrhan, G.: 'A photovoltaic module thermal model using observed insolation and meteorological data to support a long life, highly reliable module-integrated inverter design by predicting expected operating temperature'. IEEE Energy Conversion Congress and Exposition, 2009 (ECCE 2009), San Jose, CA, USA, 2009, pp. 3343–3349

[5] Killi, M., Samanta, S.: 'Modified perturb and observe MPPT algorithm for drift avoidance in photovoltaic systems', *IEEE Trans. Ind. Electron.*, 2015, **62**, pp. 5549–5559

[6] Yeung, R.S.-C., Chung, H.S.-H., Tse, N.C.-F., *et al.*: 'A global MPPT algorithm for existing PV system mitigating suboptimal operating conditions', *Sol. Energy*, 2017, **141**, pp. 145–158

[7] Patel, H., Agarwal, V.: 'Maximum power point tracking scheme for PV systems operating under partially shaded conditions', *IEEE Trans. Ind. Electron.*, 2008, **55**, pp. 1689–1698

[8] Ishaque, K., Salam, Z.: 'A review of maximum power point tracking techniques of PV system for uniform insolation and partial shading condition', *Renew. Sustain. Energy Rev.*, 2013, **19**, pp. 475–488

[9] Walker, G.: 'Evaluating MPPT converter topologies using a MATLAB PV model', *J. Electron. Eng.*, 2001, **21**, pp. 49–56

[10] Tajuddin, M.F.N., Arif, M.S., Ayob, S.M., *et al.*: 'Perturbative methods for maximum power point tracking (MPPT) of photovoltaic (PV) systems: a review', *Int. J. Energy Res.*, 2015, **39**, pp. 1153–1178

[11] Sharaf, A.M., Ismail, A., El-Khatib, R.A., *et al.*: 'A photovoltaic utilization system with bang–bang self-adjusting maximum energy tracking controller', *Int. J. Energy Res.*, 1998, **22**, pp. 1091–1098

[12] Ishaque, K., Salam, Z.: 'A deterministic particle swarm optimization maximum power point tracker for photovoltaic system under partial shading condition', *IEEE Trans. Ind. Electron.*, 2013, **60**, pp. 3195–3206

[13] Chaouachi, A., Kamel, R.M., Nagasaka, K.: 'A novel multi-model neuro-fuzzy-based MPPT for three-phase grid-connected photovoltaic system', *Sol. Energy*, 2010, **84**, pp. 2219–2229

[14] Tang, S., Sun, Y., Chen, Y., *et al.*: 'An enhanced MPPT method combining fractional-order and fuzzy logic control', *IEEE J. Photovoltaics*, 2017, **7**, pp. 640–650

[15] Taheri, Z.S.H., Ishaque, K.: 'A novel maximum power point tracking control of photovoltaic system under partial and rapidly fluctuating shadow conditions using differential evolution'. 2010 IEEE Symp. on Industrial Electronics & Applications (ISIEA), Penang, China, 2010, pp. 82–87

[16] Ahmed, J., Salam, Z.: 'A maximum power point tracking (MPPT) for PV system using Cuckoo search with partial shading capability', *Appl. Energy*, 2014, **119**, pp. 118–130

[17] Dhimish, M., Holmes, V., Mehrdadi, B., *et al.*: 'Seven indicators variations for multiple PV array configurations under partial shading and faulty PV conditions', *Renew. Energy*, 2017, **113**, pp. 438–460

[18] Ramli, M.Z., Salam, Z.: 'Performance evaluation of dc power optimizer (DCPO) for photovoltaic (PV) system during partial shading', *Renew. Energy*, 2019, **139**, pp. 1336–1354

[19] Mitra, L., Rout, U.K.: 'Performance analysis of a new high gain dc–dc converter interfaced with solar photovoltaic module', *Renew. Energy Focus*, 2017, **19–20**, pp. 63–74

[20] Sajadian, S., Ahmadi, R.: 'Distributed maximum power point tracking using model predictive control for photovoltaic energy harvesting architectures based on cascaded power optimizers', *IEEE J. Photovoltaics*, 2017, **7**, pp. 849–857

[21] A comparison of microinverters and power optimizers [Datasheet]. Available at http://www.solaredge.com

[22] Hasan, R., Mekhilef, S., Seyedmahmoudian, M., *et al.*: 'Grid-connected isolated PV microinverters: A review', *Renew. Sustain. Energy Rev.*, 2017, **67**, pp. 1065–1080

[23] Ragonese, D., Ragusa, M.: 'Designing with the SPV1020, an interleaved boost converter with MPPT algorithm [datasheet]'. Available at http://www.st.com

[24] Boogaard, M.: 'Energy output comparison, module mismatch, Ouddorp, Netherlands', SolarEdge 2010

[25] E. Energy: 'Enphase energy value proposition: a comparison of microinverter and traditional inverter technologies. Petaluma', 2009

[26] Ishaque, K., Salam, Z., Taheri, H.: 'Simple, fast and accurate two diode model for photovoltaic modules', *Solar Energy Mater. Solar Cells*, 2011, **95**, pp. 586–594

[27] Texas Instruments: 'SM72441 programmable maximum power point tracking controller for photovoltaic solar panels' [Datasheet]. Available at http://www.ti.com

[28] Linear Technology: 'LT8490 high voltage, high current buck–boost battery charge controller with maximum power point tracking (MPPT)' [Datasheet]. Available at http://www.linear.com/LT8490

[29] Alencon Systems: 'The SPOT: Alencon's utility scale DC-DC optimizer' [Datasheet]. Available at http://www.alectris.com

[30] SolarEdge: 'SolarEdge power optimizer-module embedded solution OPJ300-LV' [Datasheet]. Available at http://www.solaredge.com

[31] Alonso, R., Roman, E., Sanz, A., *et al.*: 'Analysis of inverter-voltage influence on distributed MPPT architecture performance', *IEEE Trans. Ind. Electron.*, 2012, **59**, pp. 3900–3907

[32] Gerber, D., Biela, J.: 'Interleaving of a soft-switching boost converter operated in boundary conduction mode', *IEEE Trans. Plasma Sci.*, 2015, **43**, pp. 3374–3380

[33] Maali, E., Vahidi, B.: 'Double-deck buck–boost converter with soft switching operation', *IEEE Trans. Power Electron.*, 2016, **31**, pp. 4324–4330